Discover Applied Sciences

RESEARCH Open Access

Microstructure, phase stability, and mechanical properties of binary Ti-Mo and ternary Ti-Mo-Fe alloys for biomedical applications

Nthabiseng Abigail Moshokoa[1*], Mamookho Elizabeth Makhatha[1], Mampai Lerato Raganya[2], Nkutwane Washington Makoana[3], Maje Phasha[4] and Joseph Moema[4]

*Correspondence:
Nthabiseng Abigail Moshokoa
Nthabisengmoshokoa@gmail.com
[1]Department of Metallurgy, School of Mining and Metallurgy and Chemical Engineering, University of Johannesburg, Doornfontein Campus, Johannesburg, South Africa
[2]Advance Materials Engineering, Manufacturing Cluster, Council for Scientific and Industrial Research, Meiring Naude Road, Brummeria 0184, Pretoria, South Africa
[3]National Laser Center, Council for Scientific and Industrial Research, Meiring Naude Road, Brummeria 0184, Pretoria, South Africa
[4]Physical Metallurgy Group, Advanced Materials Division, Mintek, 200 Malibongwe Drive, Randburg 2125, South Africa

Abstract

Metastable β-Ti alloys with non-toxic and low-cost alloying elements, with high biocompatibility and improved mechanical properties, are being developed globally for biomedical applications. However, there is still limited published work on Ti-Mo and Ti-Mo-Fe alloys with high Mo content and low cost alloying element with high strength designed for biomedical applications such as vascular stents. Thus, the current study uniquely investigates the combined influence of Fe addition and theoretical methods on β stability and mechanical performance of Ti-Mo alloys with high Mo content vascular stents. Two metastable β-Ti alloys, namely, binary Ti-20Mo wt% (referred to as Alloy 1) and ternary Ti-16.5Mo-1.1Fe wt% (referred to as Alloy 2), were designed using the theoretical predictive methods such as the molybdenum equivalence (*Moeq*), the average *Bo-Md* method, and the electron-to-atom ratio (*e/a*). Microstructural characterization and tensile properties of the alloys after solution treatment at 1100 °C and quenched in ice-brine were analysed. The X-ray diffraction (XRD) patterns and optical micrographs showed stability of the β phase in both alloys due to similarity in *e/a* ratio value and a slight difference in *Moeq*. Alloy 1 showed a high ultimate tensile strength (UTS) of 920 MPa and yield strength (YS) of 906 MPa, whereas a much lower UTS of 540 MPa was observed in Alloy 2. The elastic modulus decreased from 85 GPa in Alloy 1 to 74 GPa in Alloy 2, while micro-Vickers hardness increased significantly from 353 $Hv_{0.5}$ in Alloy 1 to 428 $Hv_{0.5}$ in Alloy 2. The high strength and modulus in Alloy 1 illustrated that the alloy could be considered as a potential alloy for biomedical applications such as those in vascular stents.

Keywords Ti-Mo-Fe, Theoretical methods, Micro-structures, Tensile properties, Micro-Vickers hardness, fractography

1 Introduction

Development of Ti-based alloys for a variety of biomedical applications, such as hard tissue replacements, dental implants, cardiovascular, etc., is growing rapidly [1]. Amongst the available biomaterials, titanium (Ti) and its alloys are the most widely used orthopedic implant materials to date, more especially Ti6Al4V alloy due to its excellent

properties such a high strength, high corrosion resistance, lower elastic modulus compared to stainless steels and Co-Cr alloys [2]. However, health issues such as cytotoxicity emanating from the presence of aluminum (Al) and vanadium (V) as main alloying elements are reported to cause neuro-degenerative diseases such as Alzheimer's [3, 4]. Furthermore, the elastic modulus of 110 GPa in Ti6Al4V alloy is still much higher than the elastic modulus of the human cortical bone (30–40 GPa), leading to the stress shielding phenomenon [5]. Stress shielding effect occurs when an implant material possesses an elastic modulus much higher than that of the bone it is replacing. As a result, the bone tissue surrounding the implant material will experience much lower stress than it is used to, resulting in enhanced osteoclast activity, which is bone remodelling. Consequently, bone atrophy, which reduces bone density, eventually leads to aseptic loosening or failure [6–7].

Despite the increasing demand due to the increasing population of the elderly and number of accidents, the above-mentioned challenges limit further use of Ti6Al4V alloy in manufacturing biomedical implants [7]. Therefore, alternative metallic bio-implant materials comprised of non-toxic alloying elements such as Nb, Ta, Mo, Zr, etc., with low elastic modulus, moderate strength, and a combination of high compatibility and corrosion resistance are needed [8]. At the forefront of designing and developing such alloys, the metastable β-Ti-type alloys hold much promise. Among key requirements for a potential candidate alloy to be used as a biomaterial for the manufacturing of biomedical implants are mechanical compatibility, corrosion resistance, and chemical biocompatibility [9]. According to Cui et al., the mechanical properties of a material are influenced by the processing techniques, phases present, and microstructural constituents. Thus, it is important to pay careful attention to the design aspects when developing metastable alloys [9]. Another criterion for developing metastable β-Ti alloys is the relationship between the elastic modulus and the phase stability [1].

In recent years, Ti-Mo alloys as potential biomaterials have been studied with the emphasis on their microstructure and mechanical properties. For example, Molybdenum in titanium alloys can improve corrosion resistance, help reduce elastic modulus and enhance ductility [10]. Mo demonstrate better biocompatibility, it can stabilize the β phase thus lowering the elastic modulus, it is non-toxic (when added within acceptable concentration) and it is cheaper as opposed to alloying elements such as Nb, Ta ect. In terms of mechanical compatibility, the following studies were reported: Wang et al. investigated the microstructural characteristics and mechanical properties of Ti-10Mo, Ti-15Mo, and Ti-20Mo wt% binary alloys. The XRD analysis illustrated a completely β phase in Ti-15Mo and Ti-20Mo alloys, but the corresponding transmission electron microscope (TEM) analysis revealed the existence of fine ω_{ath} particles in Ti-15Mo and Ti-20Mo alloys. Elastic modulus was reported to be the highest in Ti-15Mo alloy (104 GPa), while Ti-20Mo showed an elastic modulus of 83 GPa. The ultimate tensile strength and yield strength were the highest in Ti-20Mo (792 MPa and 734 MPa, respectively and were significantly lower in Ti-15Mo [11].

In another study, Takemoto et al. investigated the cold workability and deformation structure of a typical Ti-xMo (x = 8, 14, and 20 wt%) alloy. In this investigation, hot-rolled and then quenched alloys were studied for phase and microstructural constituents using various techniques. XRD and TEM analyses showed the Ti-20Mo alloy was comprised of only β phase. The elastic modulus were recorded as 95, 104 and 91 GPa

respectivelly [12]. Zhou et al. investigated the microstructure and mechanical properties of Ti-10Mo and Ti-20Mo alloys cold rolled and solution treated, and quenched. In the water quenched state, the Ti-10Mo depicted $\beta + \omega_{ath}$ phases, and the cold rolled Ti-10Mo showed $\beta + \alpha''$ phases; however, the solution treated and cold rolled Ti-20Mo alloy showed only β phase. The elastic modulus of the cold-rolled alloys (Ti-10Mo and Ti-20Mo) was recorded to be 79 GPa and 80 GPa, respectively. Their corresponding ultimate tensile strength was 921 MPa and 992 MPa, while the yield strength was 412 MPa and 494 MPa, respectively. Under solution-treated conditions, the elastic modulus of Ti-10Mo and Ti-20Mo alloys was 93 GPa and 75 GPa, respectively, while the corresponding ultimate tensile strength was 731 MPa and 823 MPa, and the yield strength was 465 MPa and 428 MPa, respectively [13].

From the above reported literature studies, it can be deduced that the developed Ti-Mo alloys were able to retain the β phase and improved their mechanical properties and corrosion resistances. However, the above alloys were designed using the trial and error methods without any background of their chosen compositions or design methods and the strength of the binary alloys especially Ti-20Mo alloy is still lower as compared to the strength of Ti-6Al-4 V alloy. This pose a challenge for biomeical applications such as load bearing implants and vascular stents that requires high strength. Thus, there is still a need for design and development of more metastable Ti-alloys which can compete with Ti6Al4V alloy from a compatibility, design, and cost point of view [14]. The addition of Fe as a low cost alloying element is gaining research momentum and the reason being; Fe in small amount could have an influence in the corrosion resistance and affect the biological performance of an alloy [15–16]. Fe is a strong β phase stabilizer and effective in solid solution strengthening [17].

Metastable β-Ti-Mo-Fe alloys have been and are continuously being explored, either designed using developed theoretical predictive methods or electronic parameters. The use of theoretical predictions such as molybdenum equivalence (*Moeq*), the d-electron method where two parameters such as the average *Bo* and *Md* values are proposed [18], and the electron to atom ratio (*e/a*) proposed by Ikehata et al. [19] are the mostly used to predict the formation of phases as well as an indication of weather the elastic modulus will be high or lower. The molybdenum equivalence (*Moeq*) is an expression that represents the contribution of each alloying element towards the β phase stability when they are compared to the most effective β stabilizer, which is Molybdenum (Mo). The molybdenum equivalence concept was first proposed by Molchanova et al. [20] and it was later modified by Bania. The modified coefficient of each β-stabilizers was calculated as the ratio of the critical minimum level of β-stabilizing content of Mo, which was reported by Bania to be 10 wt% [21]. Thus, the stability of β phase in Ti alloys which is dependent on theory in other words, the weight% (wt%) of the alloying elements necessary to suppress martensitic transformation temperature (Ms) in the β-Ti alloy can be predicted by quantitative rule of *Moeq.*

The innovative d-electron concept of designing Ti alloys was experimentally proposed by Morinaga [18, 22], to provide guidelines on the selection of alloying elements and to forecast the phase stability of alloys. This method is based on the theoretical calculation of the electronic structures of titanium alloys by the discrete-variational (DV) Xα cluster method [22]. Two alloying parameters that describe alloying behaviors were obtained for a variety of elements in titanium alloys. The alloying parameters are the bond order (*Bo*)

and the metal d-orbital energy level (*Md*) [1] and [23]. Morinaga et al. and Kuroda et al. have established a theoretical two-dimensional phase stability map considering the general electronic parameters, which are proven to be promising coordinates in designing and developing Ti alloys [23]. A phase stability map (called the *Bo–Md* map) as reported in another paper by Morinaga and Abdel-Hady et al., in which the areas of α, β + α, and β type alloys are separated clearly. The stability region of the β-type alloys extends to the higher *B*o and to the lower *Md* region. The values of moduli of elasticity for these alloys decrease with increasing *B*o and *M*d values in the β-type alloys region on the *Bo- Md* map [2].

Another theoretical prediction mostly used in research studies is the electron to atom (*e/a*) ratio which is used to predict the average number of valence electron for each atom [19]. The elastic modulus of metastable β-Ti alloys is related to phase constituents as widely reported in literature [24]. According to Tiwari et al., the phase stability of metals and alloys is determined by free energy that can be attributed to the change in electronic energy or the misfit or strain energy [25]. The Hume-Rothery showed that the *e/a* ratio of metals and alloys is vital in controlling the phase stability and phase transition boundaries, where *e* is the number of free valence electrons and *a* is the number of atoms [26]. Previous work by Wang et al. and Buzatu et al. has indicated that the phase stability of Ti alloys is related to the *e/a* ratio [27–28]. The function of *e/a* ratio and the expected phase constituents diagram after water quenching as reported by Laheurte et al., illustrated that stability of the β phase in Ti alloys increases with the e/a ratio and the stability limit of a Ti alloy with a fully β phase was reported to be around 4.20 and below this value presence of other phases such as ω and α″ can occur [29]. Several researchers have designed new Ti alloys with low elastic modulus using the *e/a* method, and they reported on the relationship between e/a ratio and the phase boundary and the effect of phase constitution on the elastic modulus [27, 30]. The works of Tane et al.., Guo *et al. and* Zhao et al., showed theoretically that the Young's modulus of Ti (Zr) alloys increases with the *e/a* ratio when the *e/a* ratio is higher than 4.2, [31–32]. The relationship between the elastic modulus, phase constituents, and the *e/a* ratio as illustrated by Zhao et al. in another paper, shows that when the *e/a* ratio is between 4.07 and 4.09; beyond these values (4.10–4.19), the elastic modulus increases significantly, and below these values, the modulus starts to decrease slightly [33].

Number of literature studies are published on metastable Ti based alloys designed for biomedical applications, some designed using the afore mentioned theoretical mentods. For example, Abd-elrhman et al. investigated the compatibility and performance of new low-cost β-type Ti alloys (Ti-4.7Mo-4.5Fe at% →Ti-9Mo-5Fe wt%) using the *Bo* and *Md* method, where the alloy was predicted to be situated within the martensitic region. The hot-rolled and solution-treated alloy depicted β + α″ phase with a Young's modulus of 83 GPa and ultimate tensile strength of 974 MPa [34]. In another study, Kobayashi et al., revealed the effect of Fe addition on the microstructure formation and mechanical properties of as-quenched Ti-2.0Mo-xFe (x = 0.5, 1, 1.5 and 2 at%)→ Ti-3.93Mo-xFe (x = 0.573, 1.15, 1.72 and 2.29 wt%) and Ti-3Mo-xFe (x = 0.5, 1, and 1.5 at%)→ Ti-5.84Mo (x = 0.57, 1.13 and 1.70 wt%). The formation or presences of phases included the β + α″ in alloy with low Fe content, and the formation of β + ω was more pronounced with higher Mo and Fe content. The elastic modulus in both alloys increased significantly with an increase in Fe content [35]. Lin et al. investigated a novel Ti-Ta-Hf-Zr alloys with

promising mechanical properties for prospective stent applications by using the design methods. The as-cast alloys illustrated β and ω phases, with high tensile strength of 1172 MPa, elastic modulus of 79 GPa, elongation of 1.58% and high compression yield strength of 1158 MPa [36].

The above published literature work have illustrated that the design and development of metastable β Ti alloys for biomedical applications are widely explored. However there is still limited work on the development of alloys with low cost elements such as Fe elements, and alloys with high content of Mo that are subjected and characterized only after solution treatment process only without rolling or forging with a goal to increase the strength of a material for biomedical applications such as those in vascular stents. Based on the reasons mentioned above, the current study uniquely investigates the combined influence of Fe addtion and theoretical methods on β stability and mechanical performance of Ti-Mo alloys with high Mo content vascular stents. Microstructural analysis and mechanical properties of solution treated and water quenched binary Ti-20Mo and ternary Ti-16.5Mo-1.1Fe wt% were evaluated in this study.

2 Materials and methods

2.1 Alloy design

2.1.1 The d electron method

Equation 1 below was use to calculate the average values of bond order (*Bo*) and d-orbital energy level (*Md*) of the studied alloys. Where X_i is the atomic fraction of element *i* in an alloying element, (*Bo*)*i* and (*Md*)*i* are the values of bond order and metal d-orbital energy level for element *i*, respectively [37–38]. The values of (*Md*) and (*Bo*) are calculated using both bcc Ti and hcp Ti clusters, and they are listed in a paper by Morinaga [18]. Bond order (*Bo*) and metal *d* orbital energy level (*Md*) values of pure metals were calculated and reported by Morinaga were used to calculate the composition average values of bond order (*Bo*) and metal *d*-orbital energy level (*Md*) values of developed ternary titanium alloys [18]. The calculated *Bo* and *Md* values presented in Table 1 demonstrated that when the composition of Mo is reduced to 16.5 wt% and 1.1 wt% of Fe is added as 3rd alloying element, both the *Bo* and *Md* values decrease slightly. This could be affected by the addition of Fe, which has a smaller atomic radius and electronegativity as compared to Mo. The decrease in *Bo* and *Md* values might increase elastic modulus, thus contradicting the statement made by Kuroda et al. [2]. The phase stability map in Fig. 1, was used to map out the average value of Bo and Md of Alloy 1 and Alloy 2. According to Fig. 1, both Alloy 1 and Alloy 2 are situated in the β region, indicating that the alloys will retain β phase upon quenching from high temperature.

$$\overleftarrow{Bo} = \sum X_i (Bo)_i \text{ and } \overleftarrow{Md} = \sum X_i (Md)_i \quad (1)$$

2.1.2 The electron-to-atom ratio (e/a) method

To determine the values of *e/a* ratios for each alloy, Eq. 2 was used where: where the N_i is the number of valence electrons, and the C*i* is the atomic percentage of elements *i*.

Table 1 Designated name, composition, the calculated *Moeq*, *e/a* ratio, *Bo*, and *Md*

Designated alloy name	Alloy composition (wt%)	Moeq (wt%)	e/a ratio	Bo	Md
Alloy 1	Ti-20Mo	20.0	4.22	2.82	2.39
Alloy 2	Ti-16.5Mo-1.1Fe	19.7	4.22	2.81	2.39

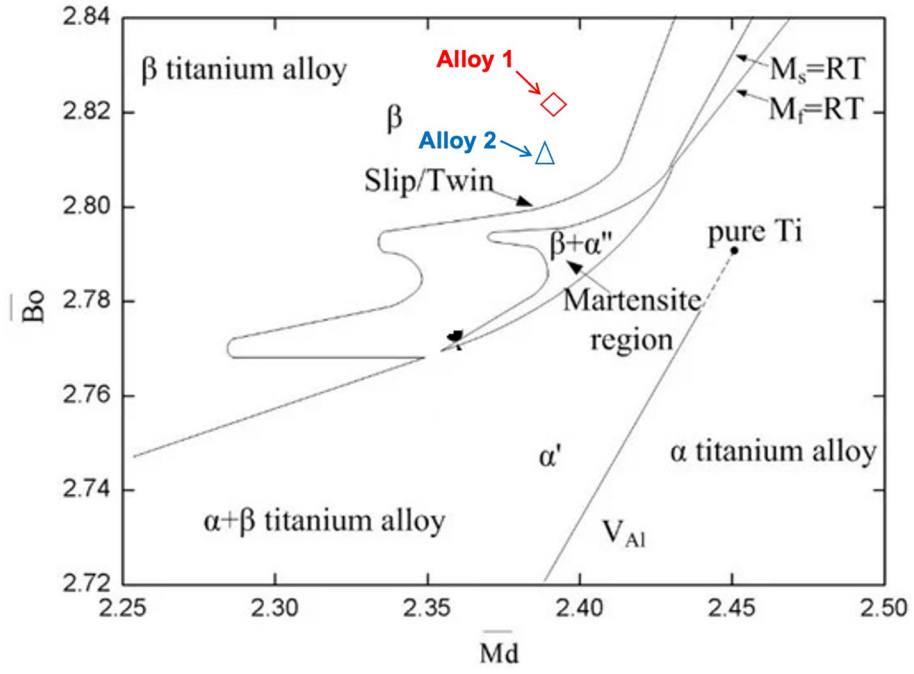

Fig. 1 Phase stability diagram based on the average *Bo* and *Md* parameters [1–2,18, 39]

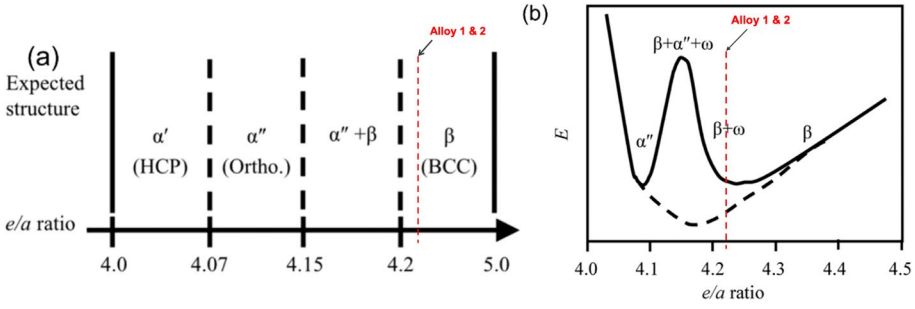

Fig. 2 Expected phase constituents in the microstructure of Ti alloys after quenching from high temperature versus e/a ratio, reproduced from Refs [29–40]. (**a**) and the relationship between elastic modulus with e/a ratio in Ti alloy systems [33] (**b**)

The calculated values are presented in Table 1 where both alloys have an equal e/a ratio of 4.22 and this predicts that they will retain the β phase upon quenching. The current work will also aid in unravelling the above discrepancy in terms of the phases present. Figure 2 illustrate the relationship between the elastic modulus, phase constituents and the *e/a* ratio. It was noticeable that both alloys are situated in the β phase reagion in Fig. 2(a) and in Fig. 2(b) they are situated in the β + ω region. According to Fig. 2 (a), both alloys are predicted to retain the β phase when characterized using XRD for example and according to Fig. 2 (b), both alloys are forecasted to form both β + ω phases upon quenching from high temperatures.

$$\overline{e/a} = \sum_{i=1}^{n} N\mathrm{i}C\mathrm{i} \tag{2}$$

2.1.3 Molybdenum equivalence (Moeq) method

The *Moeq* values of both alloys were evaluated using Eq. 3 and their values illustrated in Table 1. According to Table 1, the *Moeq* of both alloys (20.0 wt% and 19.7 wt%) are higher than 10 wt% reported by Bania, this suggest that both alloys will retain the β phase when quenched from high temperatures.

$$[Moeq]^{(B)} = 1.0\ [Mo] + 2.9\ [Fe]\ \ (wt.\%) \tag{3}$$

2.2 Experimental procedure

2.2.1 Fabrication process

The compositions of the studied alloys were varied in the following way: binary alloy with a composition of Ti-20 wt% Mo, which is designated Alloy 1, and the second alloy, designated Alloy 2, consisted of a Ti-16.5Mo-1.1Fe wt%, wherein the Mo composition was slightly lowered while a low content of Fe as a second alloying element was added. This was done to analyze the effect of simultaneous reduction and addition of Mo and Fe, respectively, on the phase constituents and mechanical properties. Titanium, Molybdenum, and Iron powders with 99.95% purity were attained from Alfa Aesar. To compact the powders into green bodies (Fig. 3a), their presented composition in Table 1 where weighed and cold compacted using a Zwick-Roell testing machine where the compaction load was 80 kN, with a cross-head speed of 20 mm/min. To further process the 50 g of compacted green bodies, the ultrasonic atomization system called the AMAZEMENT rePowder arc-melting system (Fig. 3b) which was operating under a high inert environment was used to melt the green bodies [41]. The system was purged with 100 ppm to minimise the oxygen in the chamber, a 3×10^{-1}mbar vacuum pressure was acquired for vacuuming the system, which was followed by filling the chamber with 100 mbar of pressure of argon gas. Process uses an arc with a current starting from 70 A to 270 A and temperature ranging between 100 and 2500 °C, used for melting the compacted powder on a copper hearth cooled by water that flows at 17–20 °C from the chiller. The ingot is turned more than 4 times for better homogeneity, and this is achieved by making use of a vacuum manipulator or sample gripper without opening the chamber. Melted ingots (Fig. 3c) were solution treated in a muffle furnace that was in controlled environment (Ar gas was purged in to the system before the process can begin) at 1100 °C, held for an hour, and quenched in ice-brine water. The resulting samples were thus referred to as water quenched (WQ).

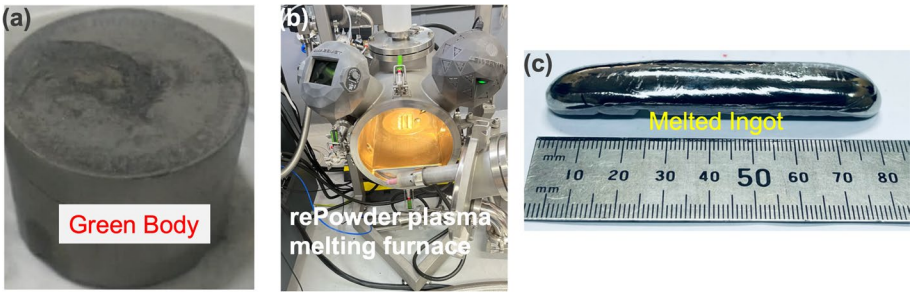

Fig. 3 Compacted green body (**a**) re-powder plasma melting furnace (**b**) [42] and melted ingot (**c**)

2.2.2 Microstructural characterization

To analyse the phase constituents in each alloy, an X-ray Diffractometer equipment called the Malvern Panalytical Empyrean was ultilized, where the Cu Kα radiation with incorporation of a secondary monochromatic (λ = 0, 1545 nm) with a voltage of 45 kV and current of 40 mA parameters were used to run the patterns. The 2θ scan range was recorded to be from 5° to 100 ° with a step size of 0.01°. For verification purposes, a reference silicon disk was conducted in the same conditions and parameters. To analyse the presence of phases, a software called the X-pert High score software was used utilized. To study the microstructural evolution, the quenched samples were prepared following the metallographic preparation standard. To reveal the microstructures and grains, the samples were etched with Kroll reagent which was composed of the following concentration: (90ml H_2O, 2 ml HF, 3 ml HNO_3, and 5 ml HCl) for 30–59 s. The DSX-HRSU Olympus (Japan) optical microscope was used to capture images at different magnifications, from low magnification of 400 µm to the highest of 100 µm. To determine elemental composition after processing and to investigate the existence of segregation, energy dispersive spectroscopy was performed in JOEL JSM-6010 Plus/LAM scanning electron microscope (SEM) at an accelerating voltage of 8 kV, where point and shoot were conducted, and the average elemental composition was recorded. Oxygen analysis of both samples were not determined in this study, however it is considered for future work. To obtain clear images with large grains, the images were taken at higher magnifications. The grain size measurements on the micrographs were conducted using ImageJ software.

2.2.3 Mechanical properties

To evaluate the mechanical properties, a tensile test method was used which it was conducted using Instron™ 1342 machine at room temperature following the ASTM E8 standard. The tensile tester machine was fitted with a 50 kN load cells and the crosshead speed was kept constant at 0.5 mm/min. Three tensile specimens per alloy with the following dimensions 40 × 5 × 3 mm were prepared using the electrical discharge machining, where a displacement was applied at a rate of 0.01 mm s^{-1}. During the test, an extensometer with 25 mm gauge length was connected to the gauge section of the test specimen with the purpose of measuring the tensile strain. The moduli were determined from the regions up to around 0.5% strain of the experimental stress-strain curves; at approximately this level of strain, then the extensometer was removed to ensure that it would not be damaged upon the sample failure. Simultaneously, and continuing above 0.5%, the strain values were recorded directly from the displacement of the universal testing machine cross heads.

Fracture surface of each alloy after tensile test was evaluated using JOEL JSM-6010 Plus/LAM scanning electron microscope (SEM) at an accelerating voltage of 8 kV, and all the images were captured at a magnification of 350 × (50 µm). To further investigate the mechanical properties, Vickers hardness of all the water-quenched samples were measured using a Zwick Roell Vickers hardness indenter machine. A small diamond was used to make indents on the samples where the load was recorded to be 500 gf and the dwell time was recorded to be 10 s. A minimum of 10 indents were made on each sample and they were evaluated microscopically and their averages were calculated.

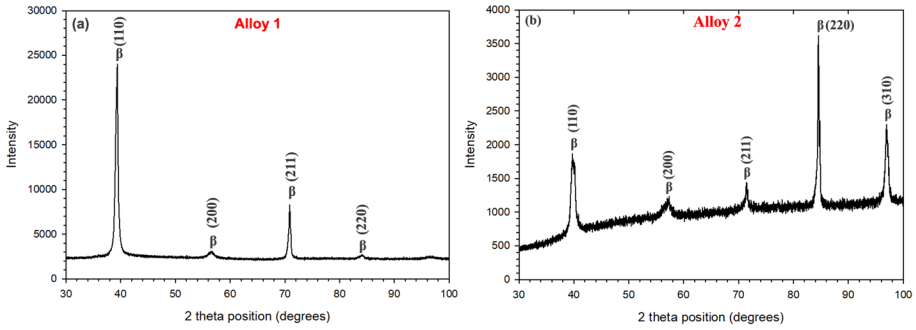

Fig. 4 XRD patterns of water-quenched (**a**) Alloy 1 and (**b**) Alloy 2 [50]

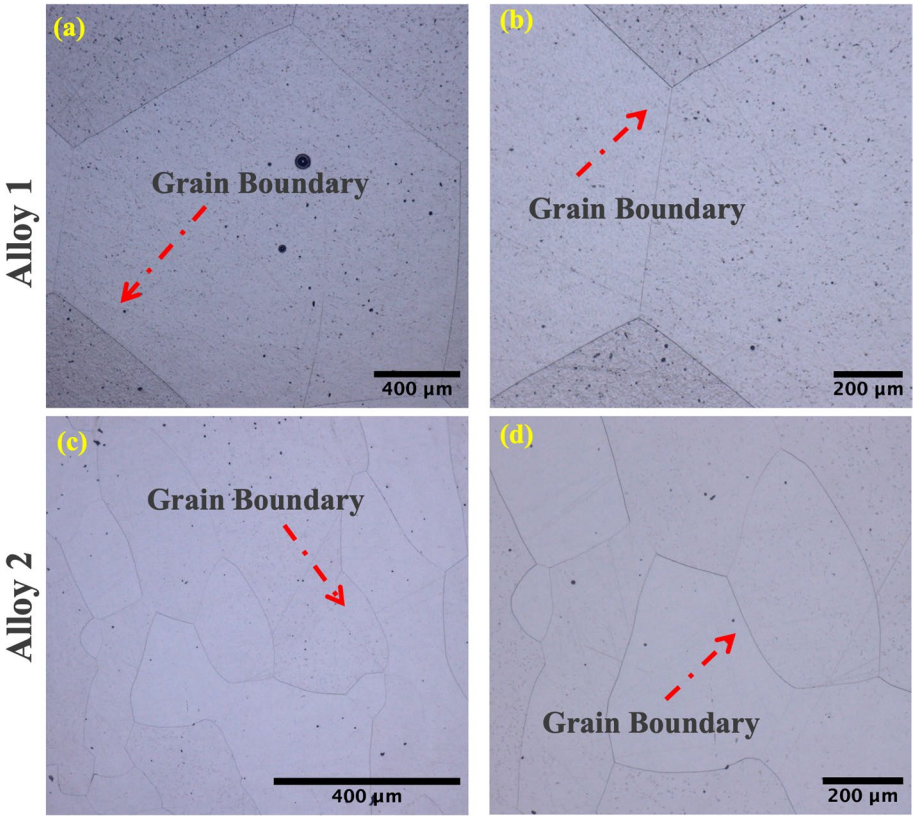

Fig. 5 OM micrographs of water quenched (**a**, **b**) Alloy 1 and (**c**, **d**) Alloy 2 [42]

3 Results and discussions

3.1 Phase and microstructural evolution

3.1.1 X-ray diffraction

Constituents' phases present in an alloy are quantified by various techniques, for which XRD is one of them. As a result, the current study deployed the XRD technique to detect phases present in the quenched alloys. XRD patterns of Alloy 1 and Alloy 2 are presented in Fig. 4(a and b), respectively. Both alloys were comprised of peaks belonging to only the β phase. The XRD peaks belonging to other phases, such as the orthorhombic (α″) and omega (ω) martensitic phases, were not detected. This absence could be ascribed to the composition, suggesting that the martensitic start transformation (Ms) temperature is below room temperature for both alloys. The Ms temperature of β-isomorphous alloys

decreases as the solute content increases [43–44]. This observation is in agreement with the previous studies [13,45]. Although the presence of an athermal omega (ω_{ath}) phase was not distinguished in the XRD patterns, this could be a result of its size falling below the detection limit of the instrument. Earlier investigations by Zhao et al. and Sabeena et al. pointed out the presence of the precipitated ω_{ath} phase in Ti-10Mo to Ti-20Mo alloys [46–47]. However, according to Sun et al. and Nakai et al., the ω_{ath} phase is difficult to detect by XRD since β and ω_{ath} phase peaks overlap [48–49].

As shown in Fig. 4(a), Alloy 1 depicted the highest peak at 2θ position of 39° belonging to the (110) plane and the lowest peak at around 2θ = 84° belonging to the (220) plane. On the other hand, Alloy 2 displayed the highest peak at 2θ = 84° belonging to the (220) plane and the shortest peak belonging to the (200) plane at a 2θ position of 57°. Phase prediction using the *Moeq* and *e/a* ratio was comparable to the experimental data. It is evident that in both alloys, the calculated *Moeq* and *e/a* ratio concurred with experimental findings, that only the β phase existed. Experimental results of Alloy 1 are similar to the ones reported by Wang et al. [11]. Due to a lack of published work with similar results as Alloy 2 after solution treatment and water quenching only, it was challenging to compare the results with the literature work.

3.1.2 Optical microscope

Micrographs of the quenched alloys were investigated using the optical microscope (OM). Figure 5depicts the OM of Alloy 1 (a) and Alloy 2 (b) in low magnification and high magnification. Both alloys exhibited β equiaxed grains without any additional structures. It was observered that the grains in the two alloys were significantly different; for instance, Alloy 1 displayed much larger grains in such a way that a single grain could not be seen when measured at higher magnification, and a clear grain with a grain boundary was visible at lower magnification. On the other hand, Alloy 2 showed distinguishable grains comprised of large and small sizes. In comparison, grains in Alloy 2 (with a grain size of 313.26 μm) were visibly observed to be much smaller than grains in Alloy 1 (with a grain size of 301.65 μm). The OM micrographs were in agreement with the XRD results in Fig. 1. The theoretical methods predicted the presence of β phase in Alloy 1 and Alloy 2, and the results agreed with the optical micrographs because there were no other structures that could be observered in the micrographs except the β equiaxed grains only. The OM micrographs of Alloy 1 are similar to the work reported by Zhou et al. [13] and Wang et al. [11]. The Optical micrographs of Alloy 2 were difficult to compare to the literature work.

3.1.3 Electron dispersive spectroscopy

Elemental distribution in both alloys after water quenching was measured using the EDS, which is incorporated in the SEM machine. The images were taken at higher magnification in both alloys, and they are presented in Fig. 6 (a and b). The point and shoot analysis was taken along the grain boundary and inside the grains in both alloys. The elemental distribution in Alloy 1 showed that Ti decreased slightly as compared to the starting material in both areas, while Mo increased slightly. The results indicated that both the grain boundary and the inside the grain were Mo-rich. Elemental distribution in Alloy 2 indicated a similar trend as in Alloy 1; both areas were rich in Mo, as the content of Mo increased significantly as opposed to the starting composition. Fe and Ti

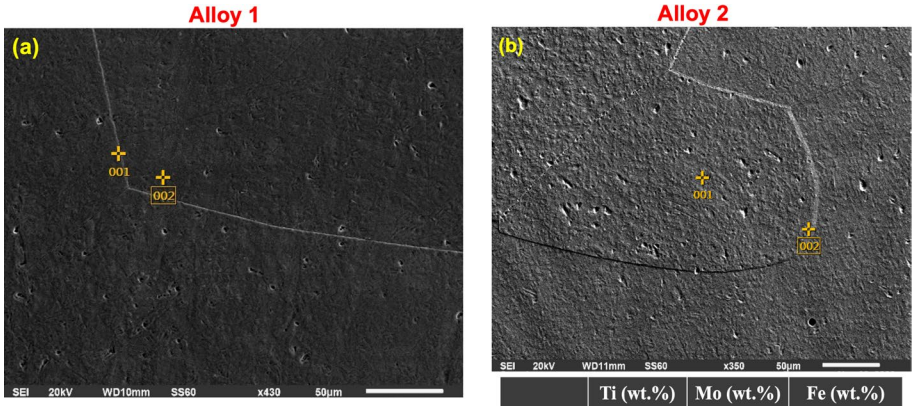

	Ti (wt.%)	Mo (wt.%)
1	79.85	20.15
2	79.52	20.48
Average	**79.69**	**20.31**

	Ti (wt.%)	Mo (wt.%)	Fe (wt.%)
1	82.20	16.81	1.00
2	80.74	18.44	0.82
Average	**81.47**	**17.63**	**0.91**

Fig. 6 EDS analysis of Alloy 1 (**a**) and Alloy 2 (**b**) after water quenching [42, 50]

Table 2 Tensile properties and Micro-Vickers hardness properties of Alloy 1 and Alloy 2

Alloy name	UTS (MPa)	YS (MPa)	E (GPa)	$Hv_{0.5}$
Alloy 1	920 ± 17.3	906 ± 11.49	84 ± 8.86	353 ± 1.98
Alloy 2	540 ± 149	540 ± 149	74 ± 7.21	428 ± 8.41

decreased notably, hence the areas were Fe and Ti-lean. The average elemental distribution in both alloys showed that segregation did occur after processing: melting and water quenching, because both alloys became rich in Mo. The studied results are consistence with the results that were reported by Ruzic et al.., in Ti-12Mo alloy [51]. To determine the content of Oxygen, further analysis will be conducted using relevant characterization techniques.

3.2 Mechanical properties

3.2.1 Tensile properties

Force related attributes such as strength, stiffness, and elongation are some of the mechanical properties that a material can include. It is vital to note that the above mentioned properties can be considered for a certain material which is appropriate for a particular application. For example, artificial joints need to be strong enough to withstand the weight and pressure of the human body [52]. The tensile properties, such as ultimate tensile strength (UTS), are represented in Table 2 below. Whereas, the YS was recorded as 906 ± 11.49 MPa for Alloy 1. Alloy 2 was brittle to produce a yield strength however, the UTS of brittle material is also considered the YS, thus the YS of Alloy 2 can be considered to be 540 ± 149 MPa. The elongation of the alloys were much lower, and this might be due to the removal of the extensometer by the operator during testing as outlined in Sect. 2.2.3. It was observed that when the Mo content was decreased and Fe added as a secondary alloying element, the UTS decreased significantly. Alloys 1 and 2 revealed UTS values of 920 ± 17.3 MPa and 540 ± 149 MPa, respectively.

It is commonly known from literature that intrinsic factors such as atomic bonding, phase evolutions, microstructural features have a bearing on the strength of a material

[53], . Four strengthening mechanisms, namely, (i) solid solution strengthening (SSS), (ii) deformation strengthening, (iii) precipitation strengthening and (iv) dispersion strengthening, as well as other microstructural factors such as grain refinement and sub-grain strengthening, can affect the strength of a material [36] and [54], . In the first three strengthening mechanisms, the strength is improved at the expense of ductility. The high strength in Alloy 1 as compared to Alloy 2 is attributed to the high Mo content in Alloy 1 as opposed to Alloy 1, indicating that the solid solution strengthening effect in Alloy 1 was higher as opposed to Alloy 2. The high strength could be due to the ductile behaviour in Alloy 1, resulting in the observed plastic deformation (the alloy yielded as opposed to Alloy 2).

On the other hand, poor plasticity in Alloy 2 (poor yield strength), resulting in lower UTS, is attributed to iron's embrittling character due to its smaller atomic size compared to the larger atomic sizes of Ti and Mo is observed in Alloy 2. A similar behaviour was recently observed in Ti-15Mo alloys containing high Fe contents of 4, 8, and 12 wt% [54]. The UTS of Alloy 1 is found to be higher compared to the Ti-20Mo alloy reported by Wang et al. [11] and Zhou et al. [13]. Furthermore, the UTS was found to be higher compared to that of the commercially available Ti6Al4V alloy. The high strength (UTS and YS) of Alloy 1 not only shows potential to be considered for the manufacturing of orthopedic implants but also for balloon expandable stents that are used in coronary vascular stents. Comparing the mechanical properties with theoretical methods, it can be deduced that the decrease in *Bo* and *Moeq* values illustrated a decrease in the strength of a material.

3.2.2 Elastic Modulus (E)

High strength is usually associated with high elastic modulus; thus, it was visible in Alloy 1, where the elastic modulus was recorded to be 84 ± 8.86 GPa, while the elastic modulus of Alloy 2 was 74 ± 7.21 GPa, as it is illustrated in Table 2 below. It is well known that the elastic modulus change with the type of phase(s) present in the alloy [55–56]. The elastic modulus is also related to the interatomic distances in the crystal lattice, which can be controlled by either alloying, heat treatment, or plastic deformation [57]. Both alloys showed the presence of β phase without the addition of other phases. Thus, the high elastic modulus in Alloy 1 is attributed to high Mo content. However, Alloy 2 demonstrated a lower elastic modulus ascribed to a substantial decrease in Mo content. A small addition of a strengthening element (Fe) could not compensate for the reduced Mo content [49, 52]. The elastic modulus of the studied alloys contradicts the predictions made by the calculated *Bo* and *Md* because Alloy 1, with the high *Bo* and *Md* values, did not show a low elastic modulus, but it was Alloy 2, with low *Bo* and *Md* values, that indicated a low elastic modulus.

The elastic modulus of Alloy 1 and Alloy 2 was much lower than that of the Ti6Al4V alloy. Although the elastic modulus of Alloy 1 was found to be higher than the modulus reported by Zhou et al. [13] and it was also higher than the modulus reported by Wang et al. [11]. The elastic modulus of Alloy 2 was lower as opposed to the following alloys (Ti-4Mo-2Fe with 84 GPa, Ti-6Mo-1Fe with 81 GPa, and Ti-6Mo-2Fe with 119 GPa), which were studied by Kobayashi et al. [35], and the elastic modulus in Alloy 2 was seen to be lower as opposed to the modulus evaluated by Min et al. [58] in Ti-5Mo-1Fe alloy with an elastic modulus of 82 GPa, and Abdel-Hardy Gepreel et al. [14,34] in

Ti-9Mo-5Fe with an elastic modulus of 83 GPa. In addition, comparing the elastic modulus in Alloy 2 and with that of commercially available TI6Al4V alloy which is 110 GPa, Alloy 2 was significantly lower. However it was noticeable that, Alloy 2 and Alloy 1 possess a high elastic modulus as compared to the cortical bone, which can be challenging for orthopedic implants because of the stress shielding effect; however, the high elastic modulus is required for balloon expandable stents used in coronary vascular stents. Thus, Alloy 1 and Alloy 2 show potential to be considered for use in balloon-expandable stents.

3.2.3 Micro-Vickers hardness (Hv)

Micro-Vickers hardness results of Alloy 1 and Alloy 2 are presented in Table 2. Hardness increased very notably from 353 ± 1.98 $Hv_{0.5}$ in Alloy 1 to 428 ± 8.41 $Hv_{0.5}$ in Alloy 2, corresponding with the addition of Fe and reduction in Mo content. According to published work, different factors such as grain size, processing techniques, cooling medium, solid solution effect, phase constituents and grain size can have an influence on the overal hardness of a material [59]. XRD detected the presence of only β phase in both alloys, though equiaxed, smaller β grains and higher grain size were observed in Alloy 2, hence higher hardness. Moreover, Furukawa et al. reported that there is a connection that can be seen between structure of a material, grain size, the distance that exist between the particles of the intermediate phases [60, 61]. The grain boundary acts as a barrier for dislocation movement and this can be explained using the Hall-petch mechanism, where dislocations find it difficult to move when the grains are smaller, however they can move easily on bigger grains. The dislocation movement and grain sizes influnces the hardness of a material: bigger grains will lead to low hardness and smaller grains will reveal higher hardness values. When compared to literature, the hardness of both alloys was notably higher compared to the Ti6Al4V alloy reported by Guo et al. [62] and higher compared to Ti-4Mo-1Fe, Ti-6Mo-1Fe wt% presented by Kobayashi et al. [35]. Hardness of Alloy 2 was found to be further higher compared to Ti-6Mo-2Fe wt% explored by Kobayashi et al. [35], and also higher than the Ti-4Mo-1Fe and Ti-6Mo-1Fe wt% alloys investigated by Abdel-hardy Gepreel et al. [14]. The relationship between strength and hardness here is that the alloy with low UTS illustrated the highest hardness due to embrittlement, and the alloy with high UTS possessed low hardness as a result of ductility. Hardness and UTS were found to be inversely proportional to each other.

3.3 Fractographic studies

The SEM micrographs of the fracture surface after the tensile test at room temperature along different orientations are depicted in Fig. 7(a to d). Generally, the degradation of metal material properties during ductile fracture is tightly related to micro damage mechanism [63]. Previous studies by Hancock et al. have illustrated two types of microfailure mechanisms: void growth and shear mechanism [64]. In void growth mechanism, the initial and new nucleated void dilate under high stress triaxiality and this lead to reduction, necking rupture on the inter-void ligaments and thus the formation of void coalescence and equiaxed dimples. In void shear mechanism, the voids elongate, rotate and interact with each other in a low and negative triaxiality region and this leads to shear localization and rupture in the inter-voids ligaments. As illustrated in [65] (a and b), irrespective of the direction of testing, the micrographs were characterized by the

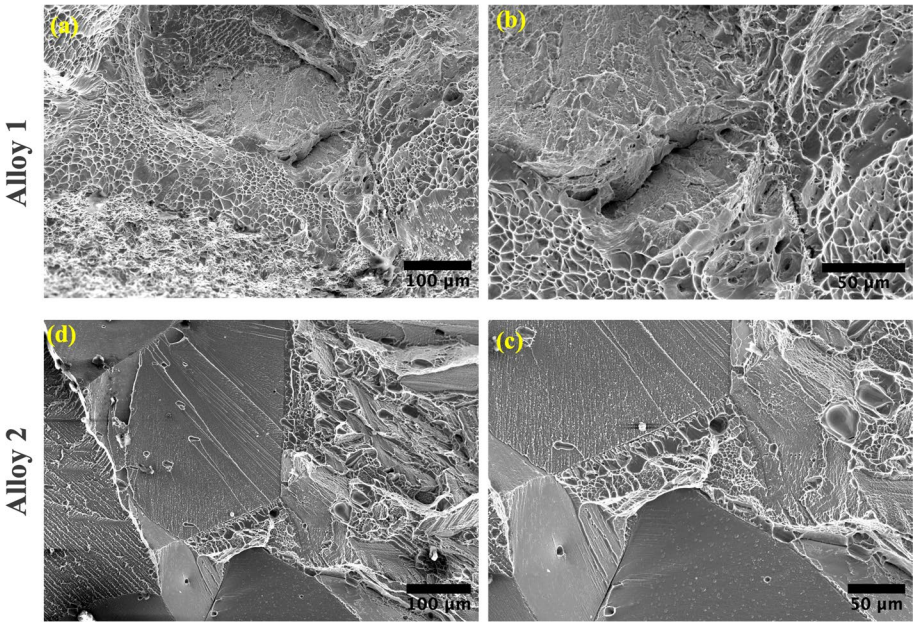

Fig. 7 Fracture surfaces of water quenched (**a** and **b**) Alloy 1 and (**d** and **c**) Alloy 2

presence of deep equiaxed fine shallow dimples indicating that the the voids have fully grown and distributed under large plastic deformation and microvoid coalescence fracture signifying ductile fracture characteristics and tearing ridges with small features of cleavage facets, which indicated that the fracture mode is a mixture of ductile fracture and cleavage fracture. Many equiaxed dimples distribute equably and present more widely and deeply due to their good plasticity of fracture [65]. Figure 7(c and d) displayed a fracture surface with large cleavage facets, coarse dimples with fewer tearing ridges, and microvoid coalescence. The appearance of coarse particle boundary facets indicated an enhanced embrittlement trend of the alloy, which ultimately leads to poor ductility due to the cleavage fracture [66]. This implies that Alloy 2 was composed of brittle fracture more as compared to ductile fracture. The results in Alloy 2 are similar to the ones reported by Nocivin et al. [67] in Ti-Nb-Zr-Fe-O alloy. The results are also similar to the fracture surface reported by [63] in Ti6Al4V alloy. The fracture surface of Alloy 1 was similar to that presented by Wang et al. [11]. and results demonstrated by [68].

3.4 Study limitation statement

The current study provides the following limitations that are considered for future work: for alloys designed for biomedical applications, biocompatibility is very vital, either mechanical, chemical compatibility ect and also further processing such as rolling, aging and annealing needs to considered. Biocompatibility can be tested in corrosion, wear properties, In vitro or in vivo test [69]. In this study mechanical test such as tensile test were conductected, however fatique test still need to be conducted and other mechanical test such as bending and compression test. Currently, corrosion and wear behaviors of Ti-Mo alloys are usually studied separately as isolated systems [20]. However, implants are generally encompassed by body fluids in the human body that induces corrosion. In vitro tests evaluate attachment, proliferation, and differentiation of osteoblasts or stem cells. Viability of fibroblasts often serves as a measure of cytotoxicity of alloys. To ascertain Ti's safety and effectiveness, it is often subjected to in-vitro cytotoxicity evaluations

using specific cell types like L929 and MC3T3 E1 cells. Through these tests, Ti's viability and reliability as an implant material are consistently demonstrated. Various studies have demonstrated the investigation of cell culture and response in metastable β-Ti alloys, for instance a Study by Mostafa et al. evaluated the in vitro and in vivo test in Ti-4.7Mo-4.5Fe and Ti-3Mo-0.5Fe alloys by using cytotoxicity test which was conducted in murine derived MCT3T3-E1 cell line for in vitro test and for in vivo, the test was done in six male V Spain while rabbits who were 6 months. The results showed that Ti-3Mo-0.5Fe alloy showed significant potential for bioactive osteogenic activity and excellent biocompatibility [70]. The literature studies show much potential for Ti-Mo-Fe based alloys to be biocompatible alloy to be considered for biomedical applications. The current study did not evaluate the corrosion resistance or cytotoxicity test of the studied composition, however the above literature pave ways for the biocompatibility test on the studied alloys to be conducted in future work.

4 Conclusions

The current study uniquely investigates the combined influence of Fe addtion and theortical methods on β stability and mechanical performance of Ti-Mo alloys with high Mo content vascular stents. The predictive methods such as *Bo* and *Md*, *Moeq* were consistent with XRD, OM results, the predicted ω phase in both alloys by *e/a* ratio method were not detectable using XRD technique, thus TEM technique is considered for future work. The tensile properties showed that the UTS and E decreased significantly when Mo decreased, while a small amount of Fe was added. The high stability of β led to improved mechanical strength elastic modulus in Alloy 1, that render it suitable for balloon-expandabel stent applications. In addition to smaller grains, the embrittling character occurring when a transition metal with a much smaller atomic radius, such as Fe, is introduced to a larger-sized Ti lattice, led to increased Vickers hardness from Alloy 1 to Alloy 2, however the strength and elastic modulus were lower. The fracture surface of Alloy 2 was composed of high fraction of dimple fracture as opposed to cleavage fracture, thus a ductile fracture. It is evident from this work that the electronic parameters are accurate in predicting the phase and microstructure of β Ti alloys. However, the atomic size difference between the solute and solvent elements plays a major role in influencing the mechanical properties thereof.

Acknowledgements
This work was supported and funded by Mintek (Advanced Metallurgy Division), and the studies were funded by CSIR-IBS. The author would like to acknowledge Mintek (AMD) and CSIR (AME and National Laser Center) for providing access to their laboratories. The author thanked colleagues at Mintek (Mr Nelson Molepo and Mr Richard Mathebula) for their assistance with experiments.

Author contributions
Nthabiseng Moshokoa: **Conceptualization of the manuscript** . Nthabiseng Moshokoa, Maje Phasha: **Methodology.** Nthabiseng Moshokoa **: Original draft preparation: ** Nthabiseng Moshokoa, Maje Phasha, Washington Makoana, Lerato Raganya, and Elizabeth Makhatha, Joseph Moema **: Software and Resources.** Moshokoa Nthabiseng and Maje Phasha **: Validation, Formal Analysis, Investigation, Data curation, Reviewing, and editing.** Maje Phasha, Elizabeth Makhatha, Lerato Raganya, Washington Makoana, Joseph Moema **: Supervision.** Elizabeth Makhatha and Maje Phasha **: Funding acquisition.** The funders had a role in the design of the study, collection of data, interpretation and analyses of data, editing of the manuscript, and the decision to publish.

Funding
We can declare that this research received no external funding.

Data availability
The data that support the findings of this study are available from the corresponding authors (Moshokoa Nthabiseng, Maje Phasha, and Elizabeth Makhatha).

Declarations

Ethics approval and consent to participate
This study does not include clinical trials or human studies, thus the ethical approval is not applicable.

Consent for publication
Not applicable.

Competing interests
The authors declare no competing interests.

Received: 29 August 2025 / Accepted: 13 March 2026
Published online: 25 March 2026

References

1. Abdel-Hady M, Hinoshita K, Morinaga M. General approach to phase stability and elastic properties of β-type Ti-alloys using electronic parameters. Scr Mater. 2006;55:477–80.
2. Kuroda D, Niinomi M, Morinaga M, Kato Y, Yashiro T. Design and mechanical properties of new i-type titanium alloys for implant materials. Mater Sci Engineering: A. 1998;243:244–9.
3. Bondy SC. Low levels of aluminum can lead to behavioral and morphological changes associated with Alzheimer's disease and age-related neurodegeneration. Neurotoxicology. 2016;52:222–9.
4. Niinomi M. Recent research and development in titanium alloys for biomedical applications and healthcare goods. Sci Technol Adv Mater. 2003;4:445.
5. Sumner DR. Long-term implant fixation and stress-shielding in total hip replacement. J Biomech. 2015;48:797–800.
6. Niinomi M, Nakai M. Titanium-based biomaterials for preventing stress shielding between implant devices and bone. Int J Biomaterials. 2011;1:pp836587.
7. Abdel-Hady Gepreel M, Niinomi M. Biocompatibility of Ti-alloys for long-term implantation. Mech Behav Biomedical Mater. 2013;20:407–15.
8. Akahori T, Niinomi M, Fukui H, Ogawa M, Toda H. Improvement in fatigue characteristics of newly developed beta-type titanium alloy for biomedical applications by thermo-mechanical treatments. Mater Sci Eng C. 2005;25(3):248–54.
9. Cui Y, Wang YW L., and, Zhang LC. Towards load-bearing biomedical titanium-based alloys: From essential requirements to future developments. Progress Mater Sci. 2024;144:101277.
10. Oliveira NTC, Aleixo G, Caram R, Guastaldi AC. Development of Ti-Mo alloys for biomedical applications: Microstructure and electrochemical characterization. Mater Sci Eng A. 2007;452–453:727–31.
11. Wang CH, Yang CD, Liu M, Li X, Hu PF, Russell AM, Cao GH. Martensitic microstructures and mechanical properties of as-quenched metastable β-type Ti–Mo alloys. J Mater Sci. 2016;51:6886–96.
12. Takemoto Y, Shimizu I, Sakakibara A, Hida M, Mantani Y. Tensile behavior and cold workability of Ti-Mo alloys. Mater Trans. 2004;45(5):1571–6.
13. Zhou YL, Luo DM. Microstructures and mechanical properties of Ti-Mo alloys cold-rolled and heat treated. Mater Charact. 2011;62(10):931–7.
14. Abdelrhman Y, Gepreel MAH, Kobayashi S, Okano S, Okamoto T. Biocompatibility of new low-cost (α + β)-type Ti-Mo-Fe alloys for long-term implantation. Mater Sci Eng C. 2019;99:552–62.
15. Ehtemam-Haghighi S, Attar H, Dargusch MS, Kent D. Microstructure, phase composition and mechanical properties of new, low cost Ti-Mn-Nb alloys for biomedical applications. J Alloys Compd. 2019;787:570–7.
16. Niu J, Guo Y, Li K, Liu W, Dan Z, Sun Z, Chang H, Zhou L. Improved mechanical, bio-corrosion properties and in vitro cell responses of Ti-Fe alloys as candidate dental implants. Mater Sci Eng C. 2021;122:111917.
17. Catanio Bortolan C, Campanelli LC, Mengucci P, Barucca G, Giguère N, Brodusch N, Paternoster C, Bolfarini C, Gauvin R, Mantovani D. Development of Ti-Mo-Fe alloys combining different plastic deformation mechanisms for improved strength-ductility trade-off and high work hardening rate. J Alloys Compd. 2022;925:166757.
18. Morinaga M. Alloy design based on the molecular orbital method. Mater Trans. 2016;57:213–26.
19. Ikehata H, Nagasako N, Furuta T, Fukumoto A, Miwa K, Saito T. First-principles calculations for development of low elastic modulus Ti alloys. Phys Rev B Condens Matter Mater Phys. 2004;70:1–8.
20. Molchanoca EK, Glazunov SG. Phase diagrams of titanium alloys. Israel Program Scientific Translations; 1965.
21. Bania PJ. Beta Titanium Alloys and Their Role in the Titanium Industry: what is a beta alloy? JOM. 1994;46:16–9.
22. Morinaga M, Yukawa N, Adachi H. Electronic Structure and Phase Stability of Titanium Alloys. Tetsu-to-Hagane. 1986;72:555–62.
23. Abdel-Hady M, Fuwa H, Hinoshita K, Kimura H, Shinzato Y, Morinaga M. Phase stability change with Zr content in β-type Ti-Nb alloys. Scr Mater. 2007;57:1000–3.
24. Zhou YL, Niinomi M. Ti-25Ta alloy with the best mechanical compatibility in Ti-Ta alloys for biomedical applications. Mater Sci Eng C. 2008;29:1061–5.
25. Tiwari GP, Ramanujan RV, Review. The relation between the electron to atom ratio and some properties of metallic systems. Mater Sci. 2001;36:271–83.
26. Hume-Rothery H, Channel Evans KM, Mabbott GW. The freezing points. Melting points and solid solubility limits of the alloys of silver and copper with the elements of the b sub-groups. Philos Trans R Soc Lond. 1934;233:1079.
27. Wang HL, Hao YL, He SY, Li T, Cairney JM, Wang YD, Wang Y, Obbard EG, Prima F, Du K, Li SJ, Yang R. Elastically confined martensitic transformation at the nano-scale in a multifunctional titanium alloy. Acta Mater. 2017;135:330–9.
28. Buzatu M, Ghica SI, Vasile E, Geanta V, Stefanoiu R, Petrescu MI, Iacob G, Butu M, Sohaciu M. On the design of new β-phase titanium alloys Ti-Mo-W. Bull Ser B. 2016;78:161–72.
29. Laheurte P, Prima F, Eberhardt A, Gloriant T, Wary M, Patoor E. Mechanical properties of low modulus β titanium alloys designed from the electronic approach. J Mech Behav Biomed Mater. 2010;3:565–73.

30. Lee SH, Todai M, Tane M, Hagihara K, Nakajima H, Nakano T. Biocompatible low Young's modulus achieved by strong crystallographic elastic anisotropy in Ti-15Mo-5Zr-3Al alloy single crystal. J Mech Behav Biomed Mater. 2012;14:48–54.
31. Tane M, Akita S, Nakano T, Hagihara K, Umakoshi Y, Niinomi M, Mori H, Nakajima H. Low Young's modulus of Ti-Nb-Ta-Zr alloys caused by softening in shear moduli c′ and c44 near the lower limit of body-centered cubic phase stability. Acta Mater. 2010;58:6790–8.
32. Guo S, Ding W, Zhang H, Lu W, Liu G, Liu H, Cheng X, Zhao X. Mechanisms of near-linear elastic deformation behavior in a binary metastable β-type Ti-Nb alloy with large recoverable strain. Mater Charact. 2022;187, 111858 .
33. Zhao J, Liu K, Ding M, Yin L, Liang S. Relationship between the composition and elastic modulus of TiZrTa alloys for implant materials. Met (Basel). 2022;12(10):1582.
34. Abd-elrhman Y, Gepreel MAH, Abdel-Moniem A, Kobayashi S. Compatibility assessment of new V-free low-cost Ti-4.7Mo-4.5Fe alloy for some biomedical applications. Mater Des. 2016;97:445–53.
35. Kobayashi S, Miyamoto A, Okano S, Abdel-Hady Gepreel M, Ibrahim MM, Ueda M, Ikeda M, Nakai K, Sakamoto T. Effect of Fe addition on the microstructure formation and mechanical properties of Ti-2.0, 3.0at%Mo alloys. Mater Sci Forum. 2014;783 :1280–1285.
36. Lin J, Ozan S, Li Y, Ping D, Tong X, Li G, Wen C. Novel Ti-Ta-Hf-Zr alloys with promising mechanical properties for prospective stent applications. Sci Rep. 2016;6(1):37901.
37. Li C, Lee DG, Mi X, Ye W, Hui S, Lee Y. Phase transformation and age hardening behavior of new Ti-9.2Mo-2Fe alloy. J Alloys Compd. 2012;549:152–7.
38. Ahmed M, Wexler D, Casillas G, Ivasishin OM, Pereloma EV. The influence of β phase stability on deformation mode and compressive mechanical properties of Ti-10V-3Fe-3Al alloy. Acta Mater. 2014;84:124–35.
39. Morinaga M, Yukawa N, Adachi H. Electronic Structure and Phase Stability of Titanium Alloys. Tetsu-to-Hagane. 1986;72:555–62.
40. Liang S. Review of the Design of Titanium Alloys with Low Elastic Modulus as Implant Materials. Adv Eng Mater. 2020;22:2000555.
41. Żrodowski Ł, Wroblewski R, Choma T, Moronczyk B, Ostrysz M, Leonowicz M, Lacisz W, Blyskun P, Wrobel JS, Cieslak G, Wysocki B, Zrodowski C, Pomian K. Novel cold crucible ultrasonic atomization powder production method for 3d printing. Materials. 2021;14:2541.
42. Moshokoa NA, Makhatha ME, Raganya L, Makoana NW, Phasha M. Phase stability and tensile properties of metastable β-Ti alloys for orthopedic applications designed using electronic parameters. J Mater Sci Mater Eng. 2025;20(1):146.
43. Davis R, Flower HM, West DR. F. Martensitic transformations in Ti-Mo alloys. Mater Sci. 1979;14:712–22.
44. Hanada S, Izumi O. Transmission Electron Microscopic Observations of Mechanical Twinning in Metastable Beta Titanium Alloys. Metall Transaction: A. 1986;17:1409–20.
45. Bagariatskii IA, Nosova GI, Tagunova TV. Factors in the formation of metastable phases in titanium-based alloys. Soviet Phys Doklady. 1958;3:1014.
46. Zhao X, Niinomi M, Nakai M, Hieda J. Beta type Ti-Mo alloys with changeable Young's modulus for spinal fixation applications. Acta Biomater. 2012;8(5):1990–7.
47. Sabeena M, Murugesan S, Anees P, Mohandas E, Vijayalakshmi M. Crystal structure and bonding characteristics of transformation products of bcc β in Ti-Mo alloys. J Alloys Compd. 2017;705:769–81.
48. Sun F, Zhang JY, Marteleur M, Gloriant T, Vermaut P, Laille D, Castany P, Curfs C, Jacques PJ, Prima F. Investigation of early stage deformation mechanisms in a metastable β titanium alloy showing combined twinning-induced plasticity and transformation-induced plasticity effects. Acta Mater. 2013;61:6406–17.
49. Nakai M, Niinomi M, Zhao X, Zhao X. Self-adjustment of Young's modulus in biomedical titanium alloys during orthopaedic operation. Mater Lett. 2011;65:688–90.
50. Moshokoa NA, Makhatha E, Raganya L, Makoana NW, Mkhonto D, Phasha M. Study of phase constituents, microstructural evolution, tensile properties and micro-Vickers hardness of as-cast and water quenched Ti-Mo-Fe alloys. Results Mater. 2026;29:100885.
51. Ruzic J, Emura S, Ji X, Watanabe I. Mo segregation and distribution in Ti–Mo alloy investigated using nanoindentation. Mater Sci Eng A. 2018;718:48–55.
52. Pal S. Design of artificial human joints & organs. Volume 1. Boston, MA: Springer US; 2014.
53. Clemens H, Mayer S, Scheu C. Microstructure and properties of engineering materials. Fundam Appl. 2017;1–20.
54. Moshokoa N, Makhatha E, Raganya L, Makoana W, Chauke H, Diale R, Phasha M. Influence of intermetallic phase (TiFe) on the microstructural evolution and mechanical properties of as-cast and quenched Ti–Mo–Fe alloys. Sci Rep. 2024;14:10461.
55. Zhou YL, Niinomi M, Akahori T. Mechanical properties of binary Ti-Ta alloys for biomedical applications. Materials Science Forum, Trans Tech Publications Ltd; 2004, pp. 1089–1092.
56. Matlakhova LA, Matlakhov AN, Monteiro SN, Fedotov SG, Goncharenko BA. Properties and structural characteristics of Ti-Nb-Al alloys. Mater Sci Engineering: A. 2005;393(1–2):320–6.
57. Sakaguchi N, Mitsuo N, Akahori T, Saito T, Furuta T. Effects of alloying elements on elastic modulus of Ti-Nb-Ta-Zr system alloy for biomedical applications. Materials Science Forum. Trans Tech Publications Ltd; 2004, pp. 1269–1272.
58. Min XH, Emura S, Nishimura T, Tsuchiya K, Tsuzaki K. Microstructure, tensile deformation mode, and crevice corrosion resistance in Ti-10Mo-xFe alloys. Mater Sci Engineering: A. 2010;527:5499–506.
59. Jamhari FI, Foudzi FM, Buhari MA, Sulong AB, Radzuan NAM, Muhamad N, Mohaned IF, Jamadon NH, Tan K. Influence of heat treatment parameters on microstructure and mechanical performance of titanium alloy in LPBF: A brief review. Mater Res Technol. 2023;24:4091–110.
60. Hall E 0. The Deformation and Ageing of Mild Steel: I1 Characteristics of the Luders Deformation. Proc Phys Soc. 1951;64:742.
61. Furukawa't M, Horita Z, Nemoto M, Valiev RZ, Langdon TG. Microhardness Measurements and the Hall-Petch relationship in Al-Mg alloy with submicrometer grain size. Acta Mater. 1996;44:4619–29.
62. Guo L, Naghavi SA, Wang Z, Varma SN, Han Z, Yao Z, Wang L, Wang L, Liu C. On the design evolution of hip implants: A review. Mater Des. 2022;266:110552.
63. Yang X, Li Y, Ge Duan M, Jiang W, Chen D, Li B. An investigation of ductile fracture behavior of Ti6Al4V alloy fabricated by selective laser melting. J Alloys Compd. 2022;890:161926.

64. Hancock JW, Mackenzie AC. On the mechanisms of ductile failure in high-strength steels subjected to multi-axial stress-states. J Mech Phys Solids. 1976;24(2–3):147–60.
65. Lu JW, Zhao YQ, Ge P, Niu HZ, Zhang YS, Zhang W, Zhang PX. Microstructure and mechanical properties of new high-strength beta-titanium alloy Ti-1300. Mater Sci Engineering: A. 2015;621:182–9.
66. Rao GA, Srinivas M, Sarma DS. Effect of oxygen content of powder on microstructure and mechanical properties of hot isostatically pressed superalloy Inconel 718. Mater Sci Engineering: A. 2006;435–436:84–99.
67. Nocivin A, Cinca I, Raducanu D, Cojocaru VD, Popovici IA. Mechanical properties of a Gum-type Ti–Nb–Zr–Fe–O alloy. Int J Min Metall Mater. 2017;24(8):909–17.
68. Kumar A, Palani IA, Yadav M. Comprehensive study of microstructure, phase transformations, and mechanical properties of nitinol alloys made of shape memory and superelastic wires and a novel approach to manufacture Belleville spring using wire arc additive manufacturing. Mater Today Commun. 2023;38:107881.
69. Bahl S, Suwas S, Chatterjee K. Comprehensive review on alloy design, processing, and performance of β Titanium alloys as biomedical materials. Int Mater Rev. 2021;66(2):114–39.
70. Mostafa D, Abdelrhman Y, Kobayashi S, Omar S, Gepreel M. Low-Cost Bio-innovative Titanium Alloys for Dental Implant Approaches (A Comparative In vitro – In vivo animal study). Egypt Dent J. 2025;71(3):2281–303.

Publisher's Note